J. Fluid Mech. (2002), *vol.* 455, *pp.* 129–148.
DOI: 10.1017/S0022112001007315 Printed in the United Kingdom

On the competition between centrifugal and shear instability in spiral Poiseuille flow

By A. MESEGUER[1] AND F. MARQUES[2]

[1]Oxford University Computing Laboratory (OUCL), Wolfson Building, Parks Road, Oxford OX1 3QD, UK

[2]Departament de Física Aplicada, Universitat Politècnica de Catalunya, Jordi Girona Salgado s/n, Mòdul B4 Campus Nord, 08034 Barcelona, Spain

(Received 18 August 2000 and in revised form 26 July 2001)

A numerical exploration of the linear stability of a fluid confined between two coaxial cylinders rotating independently and with an imposed axial pressure gradient (spiral Poiseuille flow) is presented. The investigation covers a wide range of experimental parameters, being focused on co-rotation situations. The exploration is made for a wide gap case in order to compare the numerical results with previous experimental data available. The competition between shear and centrifugal instability mechanisms affects the topological features of the neutral stability curves and the critical surface is observed to exhibit zeroth-order discontinuities. These curves may exhibit disconnected branches which lower the critical values of instability considerably. The same phenomenon has been reported in similar fluid flows where shear and centrifugal instability mechanisms compete. The stability analysis of the rigid-body rotation case is studied in detail and the asymptotic critical values are found to be qualitatively similar to those obtained in rotating Hagen–Poiseuille and spiral Couette flows. The results are in good agreement with the previous experimental explorations.

1. Introduction

In this work, we explore the behaviour of an incompressible viscous fluid contained between two concentric cylinders that can rotate independently about their common axis at constant angular velocities. An axial motion is induced in the fluid by means of an imposed axial pressure gradient. As a result, the basic flow whose linear stability will be studied is the superposition of the azimuthal Couette flow and the axial Poiseuille flow, Joseph (1976), usually termed *spiral Poiseuille flow*.

The first studies concerned with the stability of the spiral Poiseuille flow were carried out by Chung & Astill (1977) and by Hasoon & Martin (1977). In the previous explorations, the outer cylinder was assumed to be at rest. In Hasoon & Martin (1977), the perturbation fields of the basic flow were assumed to be axisymmetric and the first non-axisymmetric stability analysis was provided by Chung & Astill (1977). In a more recent numerical and experimental investigation, reported in Takeuchi & Jankowski (1981), both cylinders were rotating but the study was focused on three particular values of angular speed ratios, covering three specific cases of co-rotation, counter-rotation and outer cylinder at rest. In addition, Takeuchi & Jankowski (1981) concluded that the axial effects induced by the pressure gradient may stabilize or destabilize the basic flow depending on the sign of the angular speed ratio of the cylinders. Another conclusion from the results provided in Chung & Astill (1977) and

Takeuchi & Jankowski (1981) is that non-axisymmetric modes become dominant in the transition as long as the axial pressure gradient is increased. A comprehensive experimental study of the main features of the secondary patterns observed in the spiral Poiseuille flow has been recently provided in Lueptow, Docter & Min (1992) for the outer cylinder at rest and in a small gap geometry.

The competition between different instability mechanisms may lead to complex phenomena like stability turning points, hysteresis, multiple minima, and discontinuous changes in the critical values. Examples include the competition between buoyancy and shear in inclined natural convection, Hart (1971), between rotation and buoyancy in binary mixtures, Pearlstein (1981), between rotation and shear in Hagen–Poiseuille flow, Cotton & Salwen (1981), between buoyancy-induced shear and rotation in radial Couette flow, Ali & Weidman (1990), and between rotation and axial sliding in modulated Taylor–Couette flow, Marques & Lopez (1997). There are also examples of complicated neutral curve topology in crystal–melt interface problems as studied by McFadden *et al.* (1990). In the spiral Poiseuille problem the competition between the shear effect induced by the imposed axial pressure gradient and the centrifugal effect induced by the rotation is responsible for the aforementioned complexities.

Our study provides a first comprehensive numerical exploration of the linear stability of the spiral Poiseuille flow, covering a wide range of angular velocities of the inner and outer cylinders, both independent, and values of the axial Reynolds number. The present work is focused on the co-rotation case. One of the motivations of this particular exploration lies on the striking phenomena recently observed in a very similar problem: the *spiral Couette flow*. In the spiral Couette flow, both cylinders are rotating independently and the axial effect is induced via an inertial relative sliding between the cylinders, see Joseph (1976). As a result, shear and centrifugal instability mechanisms compete, leading to discontinuous transition Reynolds number in the critical regime. Ludwieg (1964) reported the first experimental evidence of this phenomenon and the first explanation of the mechanism of competition was provided in Meseguer & Marques (2000). As in the spiral Couette problem, the spiral Poiseuille problem also exhibits zeroth-order discontinuities in its critical surface. In both cases, this pathology has a common mathematical explanation: the spectrum of the linearized Navier–Stokes operator exhibits dramatic changes in the space of physical parameters. In other words, the spectrum may be, in both problems, split up in two independent subsets, associated with shear and centrifugal instability mechanisms. The behaviour of both subsets is independent of each other, radically swapping their dominance in the transition in co-rotating situations. When the cylinders are counter-rotating the centrifugal mechanism always dominates the axial shear.

Spiral Poiseuille flow is of importance in a number of chemical, electrical and mechanical engineering applications. The cooling of rotating electrical machinery by means of a rotor-mounted fan is but one example. An understanding of the fluid motion is needed to predict the rotor operating temperature through consideration of heat transfer to the coolant, which may increase dramatically when the centrifugal instability leads to the incidence of Taylor vortices within the laminar tangential boundary layer, Becker & Kaye (1962). In addition, a better understanding of the stability of these flows could have applications in some industrial processes like the purification of industrial waste water, Ollis, Pellizetti & Serpone (1991), the production of wire and cables, Tadmor & Bird (1974), and optical fibre fabrication techniques, Chida *et al.* (1982).

The paper is structured as follows. In § 2, the spiral Poiseuille problem is formulated mathematically. The equations are rendered dimensionless and the three dynamical

parameters R_i, R_o and Re are defined. The basic steady flow is obtained analytically assuming independence with respect axial and azimuthal coordinates. In § 3, we formulate the linear stability analysis for infinitesimal perturbations. The formulation leads to a generalized eigenvalue problem which must be solved numerically. In § 3.1, the symmetries of the linearized problem are considered in order to simplify the exploration in the space of physical parameters. A characterization of the secondary flows is provided by means of the geometrical features of the critical eigenvectors obtained from the linearized problem. From the Petrov–Galerkin formulation, a first integral of the perturbation field is obtained in order to visualize the structure of the secondary spiral flows appearing in the transition. In § 3.2, the conditions for criticality are introduced, following the same formulation used in Meseguer & Marques (2000) for the stability of spiral Couette flow. Section 4 is devoted to the numerical exploration of the linear stability. In § 4.1, we compare our numerical results with those provided in Takeuchi & Jankowski (1981), both numerical and experimental. In § 4.2, a comprehensive exploration of the co-rotating situation is presented. The numerical computations reported here were carried out for the same experimental parameters used in Takeuchi & Jankowski (1981). Section 5 is devoted to rigid-body rotation in the spiral Poiseuille problem. We compare the asymptotic critical regimes of three different flows in which shear and centrifugal mechanisms compete: rotating Hagen–Poiseuille flow, spiral Couette flow and spiral Poiseuille flow. For this purpose, a suitable axial Reynolds number is defined for the three flows in order to make the comparison meaningful from a physical point of view.

2. Formulation of the problem

We consider an incompressible fluid of kinematic viscosity v and density ρ which is contained between two concentric rotating cylinders whose inner and outer radii and angular velocities are r_i^*, r_o^* and Ω_i, Ω_o respectively. In addition, the fluid is driven by an imposed axial pressure gradient $(\partial P^*/\partial z^*) = \text{constant}$. The independent dimensionless parameters appearing in this problem are: the gap between the cylinders $d = r_o^* - r_i^*$; the radius ratio $\eta = r_i^*/r_o^*$, which fixes the geometry of the annulus; the Couette flow Reynolds numbers $R_i = dr_i^*\Omega_i/v$ and $R_o = dr_o^*\Omega_o/v$ of the rotating cylinders and the *Poiseuille* number, $P = (\partial P^*/\partial z^*)d^3/\rho v^2$, measuring the imposed axial pressure gradient.

Henceforth, all variables will be rendered dimensionless using d, d^2/v, v^2/d^2 as units for space, time and the reduced pressure (p^*/ρ^*), respectively. The Navier–Stokes equation and the incompressibility condition for this scaling become

$$\partial_t \boldsymbol{v} + (\boldsymbol{v}\cdot\nabla)\boldsymbol{v} = -\nabla p + \Delta \boldsymbol{v}, \quad \nabla\cdot\boldsymbol{v} = 0. \tag{2.1}$$

Let $\boldsymbol{v} = u\boldsymbol{e}_r + v\boldsymbol{e}_\theta + w\boldsymbol{e}_z$, the physical components of the velocity $\boldsymbol{v}$ in cylindrical coordinates (r, θ, z). The boundary conditions for the flow described above are

$$u(r_i) = u(r_o) = 0, \tag{2.2}$$

$$v(r_i) = R_i, \quad v(r_o) = R_o, \tag{2.3}$$

$$w(r_i) = 0, \quad w(r_o) = 0, \tag{2.4}$$

where $r_i = \eta/(1-\eta)$ and $r_o = 1/(1-\eta)$. The steady velocity field $\boldsymbol{v}_B$ independent of the axial and azimuthal variables that satisfies this condition is

$$u_B = 0, \quad v_B = Ar + \frac{B}{r}, \quad w_B = C\ln\left(\frac{r}{r_o}\right) + \frac{P}{4}(r^2 - r_o^2), \tag{2.5}$$

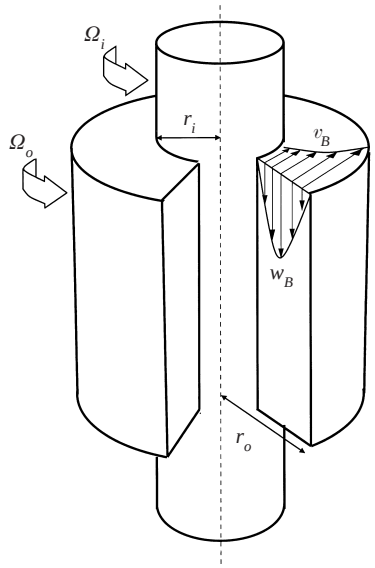

FIGURE 1. Physical description of the spiral Poiseuille problem. The basic axial–azimuthal flow is also represented.

where the constants A, B and C are

$$A = \frac{R_o - \eta R_i}{1+\eta}, \quad B = \frac{\eta(R_i - \eta R_o)}{(1-\eta)(1-\eta^2)}, \quad C = \frac{1}{\ln\eta}\frac{P(1+\eta)}{4(1-\eta)}. \tag{2.6}$$

A geometrical description of the problem can be found in figure 1. The azimuthal component of the basic flow is dictated by the Couette flow and the axial component is a superposition of logarithmic and parabolic profiles. The basic vector field $(0, v_B, w_B)$ is represented in figure 1.

Following Takeuchi & Jankowski (1981) and other previous works, we will make use of the axial Reynolds number $Re = \bar{w}d/\nu$ as a measure of the imposed axial effect, where $\bar{w}$ is the mean axial flow in the annulus,

$$\bar{w} = \frac{1}{\pi(r_o^{*2} - r_i^{*2})}\int_0^{2\pi}\int_{r_i^*}^{r_o^*} w_B^* r^* \,\mathrm{d}r^*\,\mathrm{d}\theta, \tag{2.7}$$

where w_B^* stands for the dimensional basic flow. A straightforward calculation leads to the explicit relation between the Poiseuille number and the axial Reynolds number:

$$P = \frac{8(1-\eta)^2\ln\eta}{\eta^2 - (1+\eta^2)\ln\eta - 1}Re. \tag{2.8}$$

3. Formulation of the linear stability analysis

The basic flow is perturbed by a small disturbance which is assumed to be periodic in the azimuthal and axial coordinates:

$$\boldsymbol{v}(r,\theta,z,t) = \boldsymbol{v}_B(r) + \mathrm{e}^{\mathrm{i}(n\theta+kz)+\lambda t}\boldsymbol{u}(r), \tag{3.1}$$

$$p(r,\theta,z,t) = p_B(r,z) + p'(r)\mathrm{e}^{\mathrm{i}(n\theta+kz)+\lambda t}, \tag{3.2}$$

where $\boldsymbol{v}_B = (0, v_B, w_B)$ is given by (2.5), $n \in \mathbb{Z}$, $k \in \mathbb{R}$ and $\lambda \in \mathbb{C}$. In addition, the perturbation of the velocity field must satisfy the solenoidal condition

$$\nabla \cdot [\mathrm{e}^{\mathrm{i}(n\theta + kz)} \boldsymbol{u}(r)] = 0, \tag{3.3}$$

where $\boldsymbol{u}$ must satisfy homogenous boundary conditions

$$\boldsymbol{u}(r_i) = \boldsymbol{u}(r_o) = \boldsymbol{0}. \tag{3.4}$$

Formal substitution of the perturbed fields (3.1) and (3.2) in the Navier–Stokes equations leads to the eigenvalue problem

$$\lambda \boldsymbol{u} = -\nabla p' + \Delta \boldsymbol{u} - \boldsymbol{v}_B \cdot \nabla \boldsymbol{u} - \boldsymbol{u} \cdot \nabla \boldsymbol{v}_B, \tag{3.5}$$

where the nonlinear terms have been neglected. Condition (3.3) means that the solution eigenvectors of equations (3.5)–(3.4) must satisfy the constraint

$$\left(\frac{\mathrm{d}}{\mathrm{d}r} + \frac{1}{r}\right) u + \mathrm{i}\left(\frac{n}{r} v + kw\right) = 0. \tag{3.6}$$

The boundary value problem (3.5)–(3.4), conditioned to (3.6), is numerically discretized making use of a solenoidal Petrov–Galerkin spectral method which was used in Meseguer & Marques (2000) for the stability analysis of the spiral Couette problem. The discretization leads to a generalized eigenvalue problem for the Mth order spectral approximation of the velocity field $\boldsymbol{x}_M$:

$$\lambda G(\eta, n, k) \boldsymbol{x}_M = H(R_i, R_o, Re, \eta, n, k) \boldsymbol{x}_M, \tag{3.7}$$

where $\boldsymbol{x}_M$ is given by the expression

$$\boldsymbol{x}_M(r) = \sum_{m=0}^{M} a_m^{(1)} \boldsymbol{u}_m^{(1)}(r) + a_m^{(2)} \boldsymbol{u}_m^{(2)}(r). \tag{3.8}$$

The solenoidal vector fields $\boldsymbol{u}_m^{(1)}$ and $\boldsymbol{u}_m^{(2)}$ form a basis in the space of solutions of the problem and are given by the expressions

$$\boldsymbol{u}_m^{(1)}(r) = -rkh_m(r)\, \boldsymbol{e}_\theta + nh_m(r)\, \boldsymbol{e}_z \tag{3.9}$$

and

$$\boldsymbol{u}_m^{(2)}(r) = -\mathrm{i}kf_m(r)\, \boldsymbol{e}_r + \left(\frac{\mathrm{d}}{\mathrm{d}r} + \frac{1}{r}\right) f_m(r)\, \boldsymbol{e}_z. \tag{3.10}$$

The functions f_m and h_m are combinations of Chebyshev polynomials; their detailed structure can be found in Meseguer & Marques (2000, § 3). In equation (3.7), the linear operator G depends only on the radius ratio and the axial and azimuthal wavenumbers of the perturbation. The operator H depends on the the same set of variables and on the dynamical parameters of the problem (R_i, R_o, and Re) as well. Explicit expressions for the operators G and H for a generalized axial–azimuthal basic flow $(0, v_B, w_B)$ can be found in Meseguer & Marques (2000, appendix A). The problem is then reduced to the computation of the spectrum of eigenvalues of (3.7). If, for a given set of the previous parameters, the whole spectrum lies on the left side of the complex plane, then the basic flow will be stable with respect to infinitesimal perturbations. On the contrary, if one of the eigenvalues of the spectrum has positive real part, then the basic spiral Poiseuille flow will become linearly unstable. The condition of criticality is obtained by requiring the rightmost eigenvalue of the spectrum of (3.7) to have zero real part. This condition must be imposed for each set of values of the physical and

normal mode parameters, introducing an implicit dependence between the parameters of the perturbation (n,k) and the set of Reynolds numbers (R_i, R_o, Re). Overall, the computational cost of the numerical exploration might be very high. Some advantage can be taken from the symmetries of the operators G and H in (3.7) in order to reduce the parametric exploration of the linear stability.

3.1. *Symmetries and characterization of bifurcated solutions*

Equations (2.1) are invariant with respect to the specular reflections $\{z \to -z, w \to -w\}$ and $\{\theta \to -\theta, v \to -v\}$. They are also invariant with respect to rotations around the axis, axial translations and time translations. Boundary conditions (2.2), (2.3) and (2.4) break some of these symmetries. For example, R_i or R_o different from zero breaks the specular reflection $\theta \to -\theta$, and $Re \neq 0$ breaks the specular reflection $z \to -z$. In order to keep the invariance we must change the sign of these Reynolds numbers, and of the corresponding wavenumbers n and k in the solutions of the linearized system (3.7). Obviously, the symmetries allow us to restrict the exploration to the cases $Re > 0$ and $R_i > 0$. Furthermore, since the Navier–Stokes equations are real, the complex conjugate of a perturbation (3.1), (3.2) is also a solution, and we can change simultaneously the sign of n, k and the imaginary part of λ. Therefore, the exploration in the normal mode analysis can be reduced to the case $k \geqslant 0$ and $n = 0, \pm 1, \pm 2, \ldots$.

Near criticality, the geometrical features of the bifurcated flows can be predicted from the spatio-temporal structure of the critical eigenvectors of (3.7). When axisymmetric modes, $n = 0$, are dominant in the transition, the bifurcated pattern is the Taylor vortex flow, provided that $k \neq 0$. In addition, if the imaginary part of the rightmost eigenvalue, $\omega = \operatorname{Im} \lambda$, is not zero, these Taylor vortices will travel in the axial direction with constant axial speed $c = \omega/k$. When n and k are non-zero, the eigenvector of the linear problem has the form of a spiral pattern. The wavenumbers n and k, together with ω, fix the shape and speed of the spiral. The angle α of the spiral with a z-constant plane is given by $\tan\alpha = -n/(r_o k) = -(1-\eta)n/k$; the speed of the spiral in the axial direction (on a θ-constant line) is $c = -\omega/k$, and in the azimuthal direction (on a z-constant line) it is $\omega_{sp} = -\omega/n$.

The perturbation fields defined in (3.1) are invariant under spiral-like transformations

$$\frac{\mathrm{d}z}{\mathrm{d}\theta} = -\frac{n}{k}. \tag{3.11}$$

Making use of the *spiral* coordinate $\zeta = n\theta + kz$, the solenoidal condition (3.6) can be expressed as

$$\frac{\partial}{\partial r}(ru) + \frac{\partial}{\partial \zeta}(nv + rkw) = 0. \tag{3.12}$$

Equation (3.12) implies the existence of a first integral χ of the perturbation field satisfying

$$\frac{\partial \chi}{\partial \zeta} = -ru, \tag{3.13}$$

$$\frac{\partial \chi}{\partial r} = nv + rkw. \tag{3.14}$$

From equation (3.14), and making use of the spectral approximation of the pertur-

bation field (3.8), we obtain the expression for the first integral χ_M

$$\chi_M = kr \sum_{m=0}^{M} a_m^{(2)} f_m(r), \tag{3.15}$$

provided that $k \neq 0$. The fluid particles are constrained to move in spiral isosurfaces defined by the equation

$$\mathrm{Re}\left\{ \mathrm{e}^{\mathrm{i}(n\theta+kz)} kr \sum_{m=0}^{M} a_m^{(2)} f_m(r) \right\} = \text{const.} \tag{3.16}$$

The first integral χ will be used later in order to represent the spiral component of the bifurcated solutions.

3.2. *Computation of the critical values*

In this section, we proceed to formulate the mathematical condition of criticality following the procedure used in Meseguer & Marques (2000) for the stability analysis of spiral Couette flow. Let σ be the real part of the rightmost eigenvalue of the spectrum of (3.7). For negative values of σ, the basic flow is stable under infinitesimal perturbations. When σ is zero or slightly positive, the steady flow becomes unstable and bifurcated secondary flows may appear. As mentioned before, the spectrum depends on the physical parameters and the axial and azimuthal wavenumbers of the perturbation. As a consequence, $\sigma(R_i, R_o, Re, \eta, n, k)$ is a function which implicitly depends on these variables. For fixed values of η, R_o, Re, and a (n,k)-azimuthal–axial normal mode given, the inner Reynolds number $R_i^c(n,k)$ such that $\sigma = 0$ is computed. The critical inner Reynolds number is given by $R_i^{\mathrm{crit}} = \min_{n,k} R_i^c(n,k)$, and the corresponding values of n, k are the critical azimuthal and axial wavenumbers n_{crit}, k_{crit} which will dictate the geometrical shape of the critical eigenfunction, as mentioned in § 3.1. Furthermore, the imaginary part of the critical eigenvalue, ω_{crit}, gives the angular frequency of the critical eigenfunction. Again, the critical values n_{crit}, k_{crit} and ω_{crit} are implicit functions of the parameters η, R_o and Re.

The critical condition $\sigma(k, R_i) = 0$ implicitly defines R_i as a function of the axial wavenumber k. The curve $R_i = g(k)$, usually termed the neutral stability curve (NSC), fixes the boundary between stable and unstable situations. Therefore, the critical parameter R_i^{crit} is the absolute minimum of $g(k)$ for some value $k = k_{\mathrm{crit}}$. This computation must be carried out for different values of n. As reported in Meseguer & Marques (2000), the NSC curves may have multiple extrema (maxima and minima), and exhibit disconnected parts and sharp geometrical forms. Furthermore, these curves may exhibit multivalued branches as functions of k, and these features can change abruptly in some ranges of the parameters. At this stage, we proceed to compute the critical values using a modified Newton–Raphson method the reliability of which was checked in Meseguer & Marques (2000) for the stability analysis of spiral Couette problem. The Petrov–Galerkin scheme used for the numerical approximation of the eigenvalue problem provided spectral accuracy. A convergence test of the spectral scheme can be found in Meseguer & Marques (2000, table 1).

4. Numerical results

This section is devoted to the numerical exploration of the linear stability of the basic flow. The study is focused on the co-rotation zone ($R_i R_o > 0$) and for the

Re	$Ta_L = R_i^c$	k_c	n_c	$c_l = \omega_c/k_c Re$
20	77.8415 (77.84)	3.1943 (3.19)	0	1.1778 (1.176)
70	102.6758 (102.7)	3.9501 (3.95)	4	1.8323 (1.834)

TABLE 1. Critical values for the case $\mu = 0$ and $\eta = 0.5$. The reported figures are those that apparently converged in the spectral method. The bracketed numbers correspond to the values obtained in Takeuchi & Jankowski (1981), table 1.

wide gap case $\eta = 0.5$ in order to compare our results with previous experimental and numerical data provided in Takeuchi & Jankowski (1981). Some explorations were carried out for the counter-rotating case, but the results did not provide any information not already reported in previous works. When the cylinders are rotating with opposite signs of angular speeds, the centrifugal mechanism is dominant over the axial shear, as already concluded in Meseguer & Marques (2000), where the shear was induced by a relative axial sliding between the cylinders. On the other hand, when both cylinders rotate with the same orientation, the axial shear instability mechanism may become dominant over the centrifugal one.

4.1. *Comparison with previous results*

In Takeuchi & Jankowski (1981, henceforth referred as TJ), three different explorations were carried out for different values of the rotation ratio $\mu = \eta R_o/R_i$. We have computed the critical values for the case $\mu = 0$, $R_o = 0$ in our notation, and compared with corresponding results reported by TJ in table 1; the numerical agreement is very good. The parameter $Ta = \eta R_i/(1-\eta)$ appearing in table 1 is the Taylor number, used in previous works as a measure of the angular speed of the inner cylinder, and its numerical value coincides with R_i for $\eta = 0.5$. The axial wavenumber k_c corresponds to α_L in the formulation used by TJ, where the subindex L stands for the linear critical value obtained with their numerical method. The last column of the table reports the axial speed of the bifurcated solution, $c_L = \omega/k_c Re$, based on the time-scaling considered in TJ.

In figure 2(a), we show the critical inner Reynolds number R_i^c as a function of the axial Reynolds number Re for $\mu = 0$. Our numerical computations for this case are not distinguishable from TJ's numerical results within plotting accuracy. One of the most remarkable features is that the axial effects stabilize axisymmetric as well as non-axisymmetric azimuthal modes. This stabilization is maximum at $Re \sim 60$. For larger values of Re, the stability effect decreases, eventually reversing for Re large enough. For low axial Reynolds number, the bifurcating pattern is a travelling Taylor vortex flow ($n = 0$), since $c_L \neq 0$ in the range of values of axisymmetric dominance, as reported in table 1 of TJ. As the axial effect is increased, the dominant modes become non-axisymmetric, associated with spiral secondary flows.

Our study is concerned with the computation the *absolute* instability of the spiral Poiseuille flow. The *convective* instabilities would correspond to perturbations which grow with respect to a system of reference which is moving with constant axial speed. Therefore, these kinds of disturbances undergo only a transient growth with respect to a steady system of reference, provided that they are confined to a bounded spatial domain, and they eventually decay. The comparison with the experiments is difficult since there is a spatial transient in the development of the basic axial parabolic

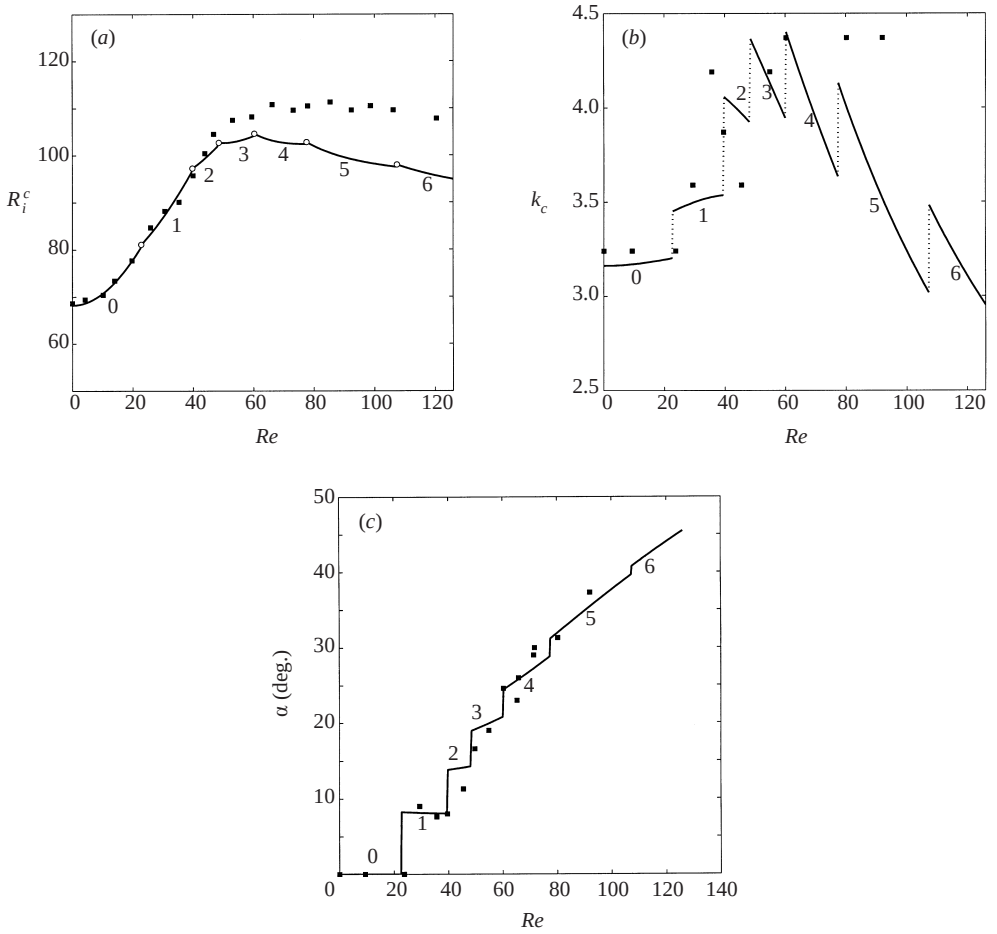

FIGURE 2. (*a*) R_i^c as a function of Re for $\mu = 0$. The circles are located at the transition between different dominant azimuthal modes, $n = 0, 1, \ldots, 6$. (*b*) Critical axial wavenumber, k_c for the same set of parameters. (*c*) Angle of the spiral pattern. The experimental results provided in Takeuchi & Jankowski (1981) are represented with black squares. Those in (*c*) were obtained from the corrigendum.

profile. The axial Poiseuille component needs a characteristic length to be completely developed and this length grows when the axial Reynolds number, Re, is increased. If the pipe is not long enough, the fluid may already have left the annular domain before the axial component of the spiral Poiseuille flow has been completely developed. As a result, what TJ observed for high values of Re was only this transient mechanism. In other words, for a fixed length of the annular pipe, there is always a threshold value of the axial Reynolds number above which the basic flow is never completely developed. A discrepancy between the numerical predicted values of transition and experimental results can be observed in figure 2(*a*), which increases with Re. In figure 2(*b*) we represent the critical axial wavenumber k_c as a function of Re for the same set of parameters. The computed angle of the bifurcated spiral pattern is plotted in figure 2(*c*) and compared with the corrected experimental data provided by TJ in their corrigendum.

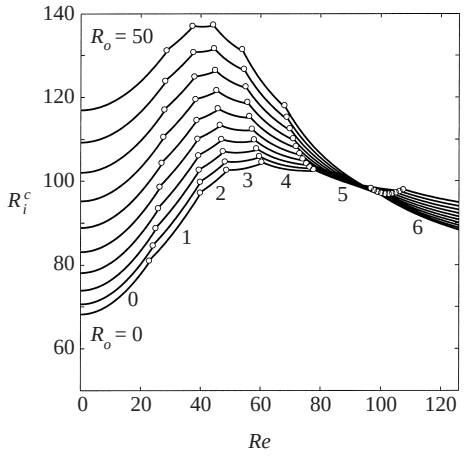

FIGURE 3. R_i^c as a function of the axial Reynolds number for low values of $R_o = 0$ (bottom), 5, 10, …, 50 (top). The dominant azimuthal modes are labelled from 0 to 6. The transitions between different azimuthal modes are represented with circles.

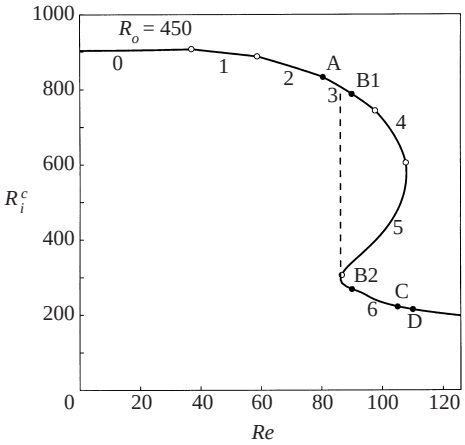

FIGURE 4. Critical curve $R_i^c(Re)$ for $R_o = 450$. The integer numbers near the curve stand for the dominant azimuthal numbers $n = 1, 2, \ldots, 6$. The circles are located at the transition point between different azimuthal modes. The dashed vertical line is located at the point of discontinuity. Points A, B1, B2, C and D correspond to figures 5(*a*) to 5(*d*), see text.

4.2. *Exploration in the co-rotation zone*

The critical behaviour for low values of R_o is qualitatively the same as for the case $R_o = 0$, previously discussed. In figure 3, we represent the critical inner Reynolds number R_i^c as a function of the axial Reynolds number Re in the range of outer rotation values $R_o \in [0, 50]$. It can be observed that the axisymmetric mode $n = 0$ is always dominant for $Re = 0$, being stabilized as Re is slightly increased from that limit value. The first non-axisymmetric modes $n = 1, 2$ are stabilized by the axial effects although $n = 3$ is only stabilized in a small range of values of R_o. Higher non-axisymmetric modes are always destabilized.

This behaviour is no longer valid for higher values of R_o. In figure 4 we plot the critical curve for $R_o = 450$. The first relevant feature is that R_i^c is almost independent of Re for axisymmetric disturbances. The first non-axisymmetric modes $n = 1$ and

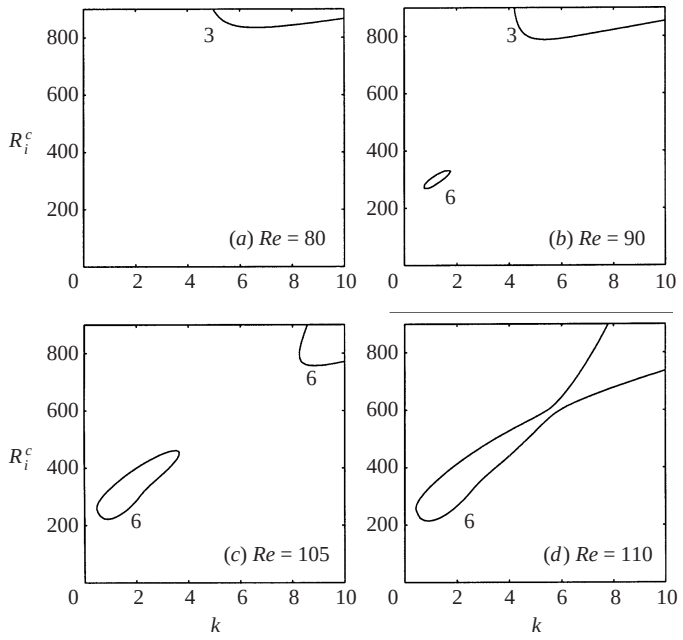

FIGURE 5. Formation of an island of instability for $\eta = 0.5$ and $R_o = 450$. The different branches are identified by their corresponding azimuthal numbers.

$n = 2$ are destabilized by the axial effect. In the range of values where $n = 3$ is dominant, the critical curve exhibits a zeroth-order discontinuity for $Re = 86.26$ (dashed vertical line) $n = 6$ being the dominant mode for higher values of Re. If we consider Re^c as a function of R_i, the critical curve is continuous and this can be used to compute the hidden branch, where the modes $n = 3, 4$ and 5 are dominant. In figure 5 we describe this phenomenon by means of the topological features of the neutral stability curves for $R_o = 450$. In figure 5(a), we represent the neutral stability curve for $n = 3$ and $Re = 80$ (point A in figure 4) where the critical value $R_i^c = 832.3$ is reached for $k_c = 6.55$. For $R_o = 90$ (figure 5b), the centrifugal mode $n = 3$ has a critical value $R_i^c = 787.2$ (point B1, figure 4) but the shear mode $n = 6$ develops an island of instability whose minimum is located at $k_c = 0.892$ and $R_i^c = 235.6$, thus being dominant (point B2, figure 4). For $R_o = 105$, the island of instability has grown in size (figure 5c) with a critical Reynolds number $R_i^c = 221.3$ (point C, figure 4). For $R_o = 110$, the neutral stability curve associated with the shear mode becomes connected (figure 5d) with a minimum value $R_i^c = 213.5$ (point D, figure 4). In order to detect these topological anomalies as soon as they appear, a modified Newton–Raphson method already formulated in Meseguer & Marques (2000) has been used.

For fixed values of R_o and Re, three different spiral regimes can be observed in the transition, depending on the value of the inner rotation Reynolds number R_i. In figures 6, 7 and 8 the essential features of the three different spiral regimes along the folded critical curve $R_o = 450$ for a fixed axial Reynolds number $Re = 100$ are depicted. The first plot (a) shows isolines of the first integral χ, computed from equation (3.16), in the (r, z)-plane; these curves are sections of the χ isosurfaces where the particles are constrained to move. The second plot (b) shows isolines of v_θ, which provides the complete structure of the spiral once χ is given. Both these representations

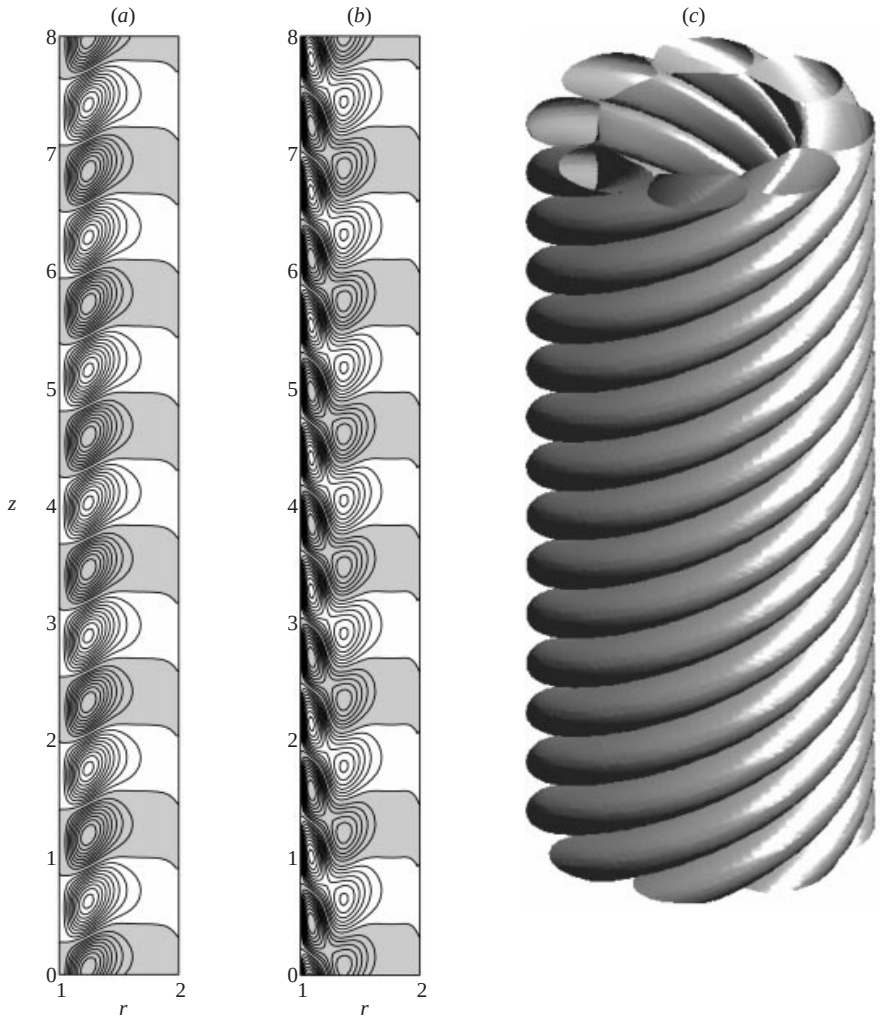

FIGURE 6. (*a*) Radial-axial cross-section of χ-eigenmode (*b*), azimuthal component of the velocity field v_θ and (*c*) three-dimensional representation of a $\chi = \text{const}$ isosurface. In (*a*) and (*b*), shaded regions correspond to negative values of the represented variable. Centrifugal branch: $R_o = 450$, $Re = 100$, $R_i^c = 722.9$, $k_c = 5.549$ and $n_c = 4$.

have been done using the same radial–axial aspect ratio in order to emphasize the characteristic length of the spiral regime in each case. Finally, plot (*c*) is which a three-dimensional visualization of one of the $\chi = \text{const}$-isosurfaces which provides a better understanding of the secondary pattern. In all three plots, we have depicted only the eigenfunction corresponding to the critical eigenvalue, omitting the basic flow. For the spiral Poiseuille problem, the basic flow contributes a constant factor to the χ first integral, leaving the mean geometric features of the spirals invariant. In figure 6 the spiral regime corresponding to the centrifugal branch is represented, where the critical azimuthal value is $n_c = 4$ and $R_i^c = 722.9$. In this case, the angle of the spirals is very low, $\alpha \sim 20^\circ$, and the highest gradients in the azimuthal velocity v_θ are mainly concentrated near the inner radius, where the centrifugal effects are more dominant. Also, the azimuthal speed is very low in the medium gap and near the

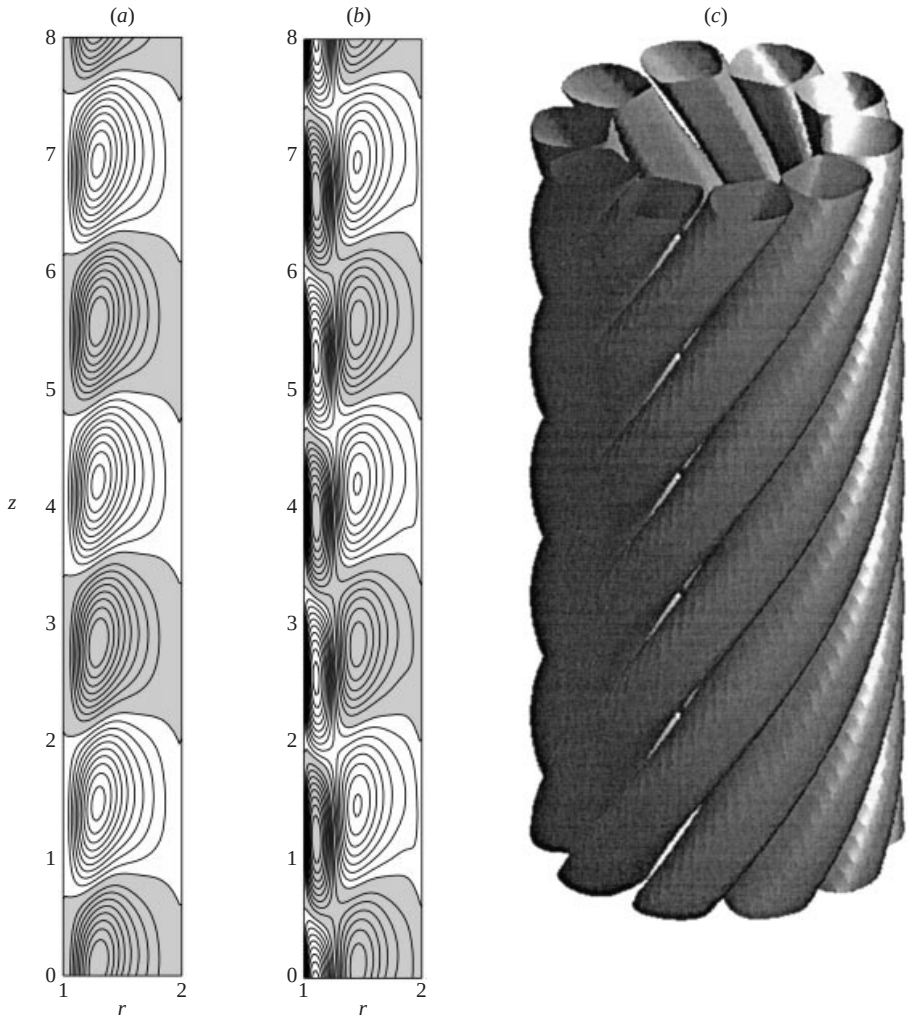

FIGURE 7. Same as figure 6 for the hidden branch: $R_o = 450$, $Re = 100$, $R_i^c = 415.4$, $k_c = 2.293$ and $n_c = 5$.

outer wall. The hidden branch is represented in figure 7, where the azimuthal mode is $n_c = 5$ and $R_i^c = 415.4$. In this branch, the angle of the spirals has increased to $\alpha \sim 48^\circ$ and the distribution of azimuthal component of the velocity has spread to the whole gap. Finally, in figure 8 we plot the spiral pattern corresponding to the shear branch, for $n_c = 6$ and $R_i = 232.2$. The spirals are almost parallel to the axis in the last case, with an approximate angle of $\alpha \sim 74^\circ$.

Figure 9 summarizes the behaviour of R_i^c for different values of R_o; we represent the critical curves of the co-rotating spiral Poiseuille flow in the range $R_o \in [0, 450]$ and $Re \in [0, 125]$. In figure 10 we represent the critical surface where the folding can be better visualized. The curve corresponding to the numerical results obtained in TJ for the particular co-rotating case $\mu = 0.2$ is also plotted in order to emphasize that their explorations were carried out far away from the cuspidal zone where the discontinuities may appear. A two-dimensional projection of the transition curves between different azimuthal modes is plotted in figure 11; the projections of the

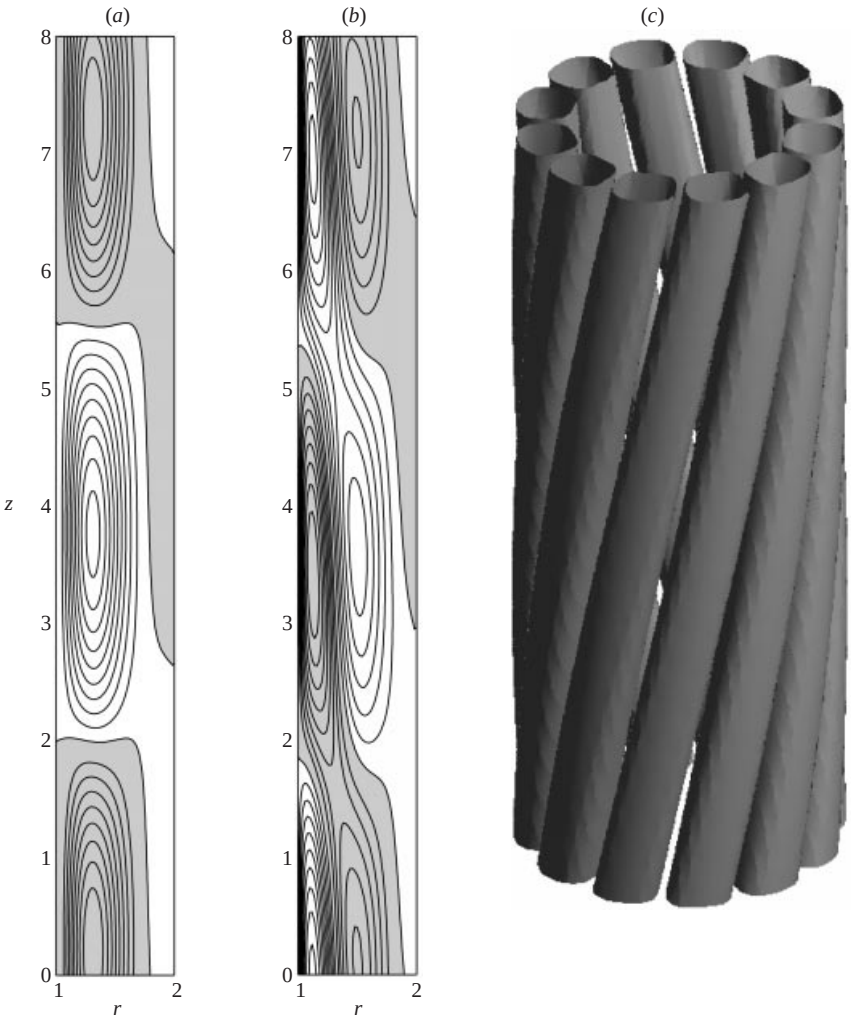

FIGURE 8. Same as figure 6 for the shear branch: $R_o = 450$, $Re = 100$, $R_i^c = 232.2$, $k_c = 0.888$ and $n_c = 6$.

maxima and minima of the folded surface are represented by dashed lines. These two curves are the boundaries of the cuspidal zone where the discontinuities may appear and they merge at the cuspidal point of coordinates $R_o = 243.1$, $Re = 80.35$.

Some similarities can be pointed out between the critical surface of the spiral Poiseuille problem and the one obtained in Meseguer & Marques (2000) for spiral Couette flow. First, the axisymmetric mode is always dominant for small values of Re and the critical value R_i^c is almost independent of the axial effect as the outer rotation number R_o is increased. Second, the threshold value of the axial Reynolds number in the cuspidal zone of the spiral Couette flow was $Rz = 73.41$ which is agreement with that obtained for the cuspidal point of the spiral Poiseuille flow within 9% relative error, Meseguer & Marques (2000). The range of dominant azimuthal modes is slightly wider in the spiral Poiseuille flow. This phenomenon can be explained in terms of the *effective* gap of the problem. In the next section, we will see that the shear effect of a spiral Poiseuille flow with $\eta = 0.5$ is qualitatively equivalent to the

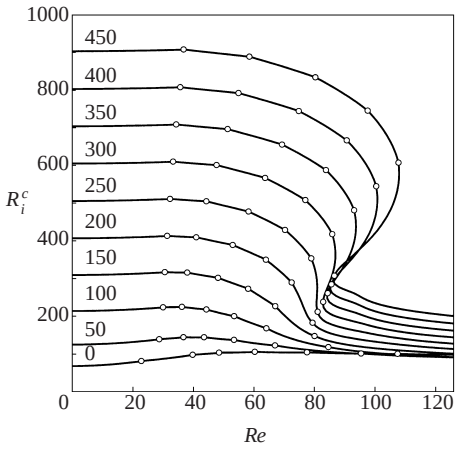

FIGURE 9. Critical curves R_i^c as a function of the axial Reynolds number Re for $R_o = 0, 50, 100, \ldots, 450$. The circles are located at the transition between different azimuthal modes n.

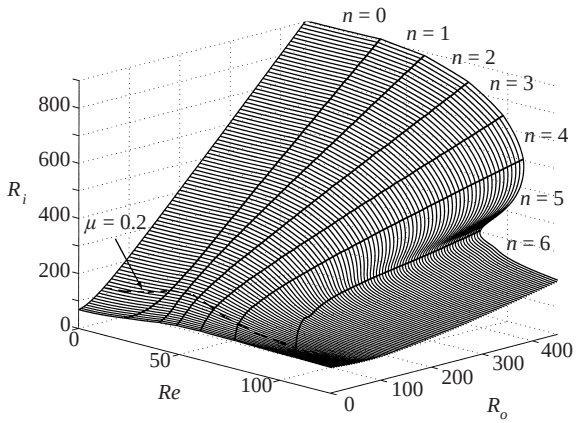

FIGURE 10. Three-dimensional representation of the critical surface for the spiral Poiseuille flow. The labels $n = 0, \ldots, 6$ are located in the zones of dominance of different azimuthal modes whose boundaries are depicted by thicker lines. The arrow indicates the curve where the computations for the case $\mu = 0.2$ were carried out in Takeuchi & Jankowski (1981).

shear effect produced by a spiral Couette flow with effective radius ratio $\eta_{\text{eff}} \sim 0.73$. As the radius ratio approaches the unity, the axial shear effect becomes more and more dominant and the range of dominant azimuthal modes increases rapidly, as already concluded in Meseguer & Marques (2000) and Ludwieg (1964) for the small gap case $\eta = 0.8$ in spiral Couette flow.

In figure 12(a) we plot the axial speed of the spirals, $c = -\text{Im}(\lambda/k)$, for different values of the outer rotation Reynolds number R_o as a function of the axial Reynolds number Re. The speed of the spirals increases dramatically above the threshold Reynolds number $R_o = 243.1$, where the shear mechanism becomes dominant. This is reflected in the plot for the curves $R_o = 300$ and $R_o = 400$, where the discontinuity appears. In the shear branch, the axial speed of the spirals is increased by approximately 60% with respect to the centrifugal speed. The authors had observed this already in the behaviour of the spirals in spiral Couette flow, where the relative increase of the axial speed of the spirals was even bigger. For low values of the axial

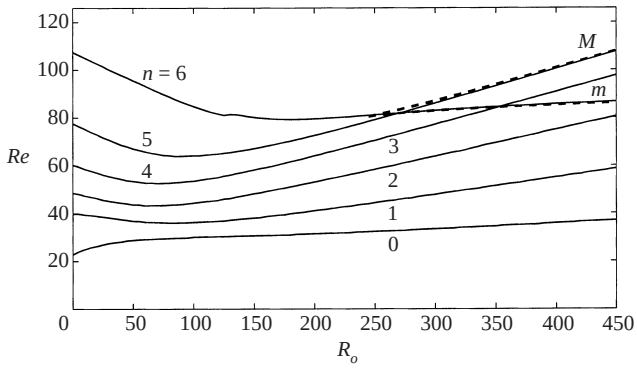

FIGURE 11. Projection of the transition curves between different critical azimuthal modes in the plane (Re, R_o). The dashed lines m and M are the projection of the minima and maxima of the folding surface respectively and are the boundaries of the cuspidal zone.

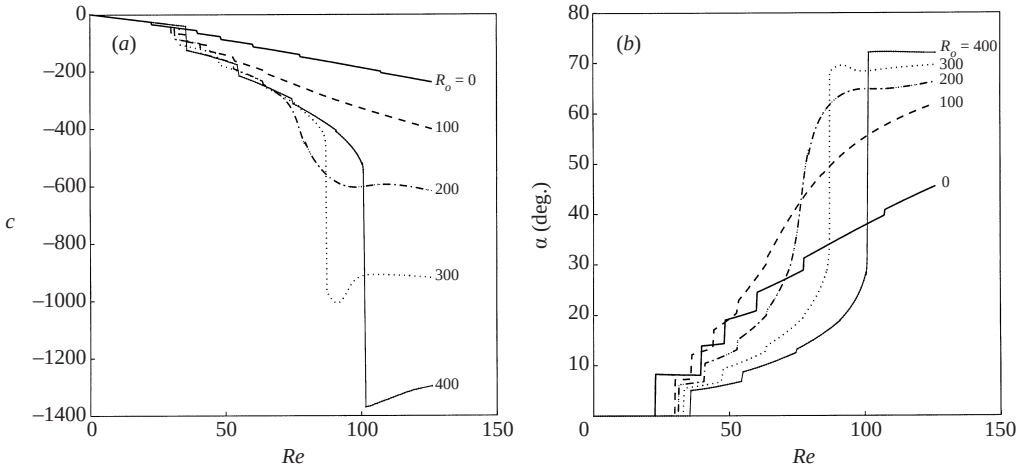

FIGURE 12. (a) Axial speed of the spiral pattern c as a function of Re, for different values of R_o. (b) Angle of the spiral pattern.

Reynolds number Re the speed of the spirals increases almost linearly with respect to Re. In particular, for $Re \neq 0$, the secondary solution is always advected downstream with a non-zero axial speed. This is in contrast with the behaviour of spirals in spiral Couette flow, where the secondary solutions were almost steady for low axial Reynolds number, see Meseguer & Marques (2000), figure 7(d). In figure 12(b), the angle of the bifurcated spiral pattern is plotted as a function of the two Reynolds numbers. In the shear branch, the spirals become almost parallel to the axis of the cylinders, with angles between 70° and 80°. After the cuspidal zone has been crossed, the spirals reach an asymptotic regime where their angles are almost independent of the axial Reynolds number Re.

5. The rigid-body rotation: overview

This section is devoted to the linear stability of spiral Poiseuille flow in the particular case of both cylinders rotating with the same angular speed Ω, which is equivalent to considering a linear dependence between the inner and outer rotation Reynolds

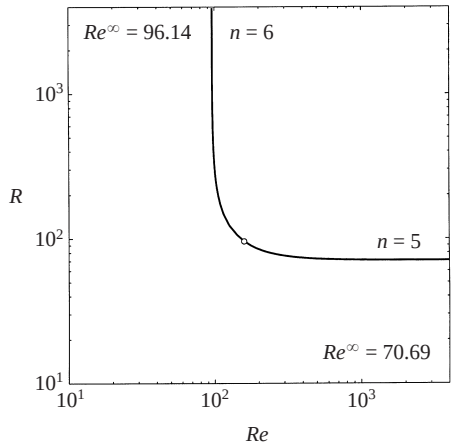

FIGURE 13. Asymptotic regimes of the rigid-body rotation of the spiral Poiseuille flow. The circle is located at the transition between the azimuthal modes $n = 5$ and $n = 6$.

numbers $R = R_i = \eta R_o$. In Meseguer & Marques (2000), the same problem was studied for spiral Couette flow. In both cases, asymptotic values of the critical regime have been obtained for high rotation rate R or high axial Reynolds number Re. In Mackrodt (1976), a study of the stability of Hagen–Poiseuille flow (pipe flow) with imposed rotation was reported, and those asymptotic regimes were computed. Mackrodt showed that, although Hagen–Poiseuille flow is linearly stable for any axial Reynolds number, the superposition of a slow rotation of the pipe may destabilize the basic flow. And conversely, although the rigid-body rotation flow is linearly stable for any angular speed, the superposition of a finite axial effect destabilizes the basic flow. The same mechanism was observed in the spiral Couette flow between coaxial cylinders rotating with the same angular speed. In the spiral Couette problem, the axial effect was introduced by means of a relative axial sliding of the cylinders. For this case, it was observed that the rigid-body rotation was stable in the absence of axial effects. Correspondingly, the axial sliding flow was always stable when the rotation was absent. In both cases the superposition of shear and centrifugal mechanisms made the basic flow unstable. In figure 13, we plot the critical curve for the rigid-body spiral Poiseuille flow. As in rotating Hagen–Poiseuille and spiral Couette flows, two asymptotic regimes are found to be dominant: for high values of the rotation Reynolds number R, finite Re, and for high values of the axial Reynolds number Re, finite R. As the rigid-body rotation is increased, the critical curve reaches an asymptotic value for $Re^{\infty}_{\text{centrif}} = 96.14$, where the azimuthal mode in the transition is a spiral regime $n = 6$ (centrifugal branch). When the axial effect is increased to high values, the critical rigid-body rotation number R tends to an asymptotic value $R^{\infty}_{\text{shear}} = 70.69$ (shear branch), $n = 5$ being the dominant azimuthal mode.

In order to make a comparative analysis of the rigid-body rotation among rotating Hagen–Poiseuille, spiral Couette and spiral Poiseuille problems, a suitable control parameter for the axial shear effect needs to be properly defined. In Mackrodt (1976), the axial Reynolds number for rotating Hagen–Poiseuille flow, Re_{HP}, was obtained in terms of the maximum value of the basic flow attained at the axis of the pipe. In Meseguer & Marques (2000), the axial Reynolds number Re_{SC} for spiral Couette flow was obtained using the axial speed of the inner cylinder which coincides with the maximum axial velocity of the logarithmic profile in the basic flow. As mentioned in

the introduction, we have considered the axial mean flow speed as a measure of the axial effect in the spiral Poiseuille problem. We adopted this convention following TJ and other previous works. Nevertheless, in this section we shall consider an alternative definition of the axial Reynolds number for spiral Poiseuille flow. The *effective* axial Reynolds number is given by

$$Re_{\text{eff}} = \frac{U^M d_{\text{eff}}}{\nu}, \tag{5.1}$$

where U^M is the maximum axial dimensional speed of the basic flow and d_{eff} is the effective gap

$$d_{\text{eff}} = r_o^* - r_M^*, \tag{5.2}$$

which is the difference between the dimensional external radius r_o^* and the value r_M^* at which the axial speed is maximum. In Mackrodt (1976) and Meseguer & Marques (2000), the Reynolds numbers Re_{HP} and Re_{SC} were the effective values respectively since the maximum axial speeds were attained at the inner radius r_i in both cases. For spiral Poiseuille flow this is no longer valid and we have to consider the maximum speed w_B^M of the axial basic flow (2.5) attained at $r = r_M$,

$$w_B^M = w_B(r_M) = \frac{2(1-\eta)^2 \ln\eta}{\eta^2 - (1+\eta^2)\ln\eta - 1}\left[\frac{1+\eta}{(1-\eta)\ln\eta}\ln\left(\frac{r_M}{r_o}\right) + r_M^2 - r_o^2\right] Re, \tag{5.3}$$

where

$$r_M = \left[-\frac{1+\eta}{2(1-\eta)\ln\eta}\right]^{1/2}. \tag{5.4}$$

For the wide gap case $\eta = 1/2$, the numerical values of the previous expressions are

$$w_B^M = \frac{\ln(27/2\ln^3 2) - 3}{\ln(32) - 3} Re \sim 1.5078\, Re \tag{5.5}$$

and

$$r_M = \left[\frac{3}{\ln 2}\right]^{1/2} \sim 1.4711, \tag{5.6}$$

very close to the mid gap value $(r_i + r_o)/2 = 3/2$. The corresponding effective radius ratio is

$$\eta_{\text{eff}} = \frac{r_M}{r_o} = (1-\eta)\left[-\frac{1+\eta}{2(1-\eta)\ln\eta}\right]^{1/2}. \tag{5.7}$$

The effective axial Reynolds number Re_{SP} is obtained from (5.1), the value of w_B^M in (5.3) and the value of d_{eff} obtained in (5.2):

$$Re_{SP} = w_B^M \frac{d_{\text{eff}}}{d} = w_B^M \frac{1-\eta_{\text{eff}}}{1-\eta}. \tag{5.8}$$

For $\eta = 1/2$, the effective radius ratio has an approximate value of $\eta_{\text{eff}} \sim 0.7355$ and the axial Reynolds number obtained from the mean axial flow and the effective one are related as follows:

$$Re_{SP} \sim 0.8035\, Re. \tag{5.9}$$

As a result, the axial mean flow of the spiral Poiseuille problem contributes only 80% approximately to the shear mechanism when it is compared with Re_{HP} and Re_{SC}. Therefore, the asymptotic value $Re^\infty = 96.14$ for the centrifugal branch should be

	Re_{eff}^{∞}	$\lvert n_s \rvert$
Rot. Hagen–Poiseuille	82.88	1
Spiral Couette	85.11	5
Spiral Poiseuille	77.26	6

TABLE 2. Threshold asymptotic values of the rigid-body rotation flow for rotating Hagen–Poiseuille flow, from Mackrodt (1976), spiral Couette flow, from Meseguer & Marques (2000), and spiral-Poiseuille flow, with the normalization explained in § 5. The first column reports the effective axial Reynolds number. The second column contains the dominant azimuthal value $|n_s|$ in the shear asymptotic branch.

renormalized to an effective value $Re_{SP}^{\infty} = 77.26$. Table 2 summarizes the asymptotic threshold values for the three flows. The agreement between the three asymptotic axial Reynolds numbers Re_{HP}, Re_{SC} and Re_{SP} is quite good, with a maximum relative discrepancy of 5%.

6. Conclusions

A comprehensive exploration of the stability of spiral Poiseuille flow has been presented and remarkable new features have been found in the critical regime. First, the presence of islands of stability in the neutral stability curves is found to be responsible for the discontinuities in the critical surface and the associated zeroth-order discontinuities in the critical Reynolds number R_i^c. Second, the competition between shear and centrifugal mechanisms of instability leads to a cuspidal region in co-rotating situations where complex dynamics including hysteresis and mode competition is likely to occur.

The characterization of the bifurcating eigenfunctions was carried out in detail, particularly in the cuspidal region. The existence of a first integral for the particles trajectories is used to visualize the bifurcating pattern near the critical points. Striking differences are found between the bifurcating spiral structures in the shear, centrifugal and hidden branches along the folded critical surface. The numerical results are in good agreement with the currently available experimental data. Nevertheless, some discrepancies appear as the axial effect is increased. This anomaly is apparently due to finite length effects in the experiment as well as to visualization techniques.

The rigid-body rotation is reviewed in detail for three prototype flows where the centrifugal and shear mechanisms compete: rotating Hagen–Poiseuille flow, spiral Couette flow and spiral Poiseuille flow. A suitable axial Reynolds number for the three flows is defined in order to make such comparison. The asymptotic threshold values for instability in the shear branch appear to be qualitatively similar despite the different nature of the three problems.

Overall, the instability mechanisms of spiral Poiseuille flow are qualitatively similar to the ones observed in our analysis of spiral Couette flow (Meseguer & Marques 2000). Nevertheless, new experiments are needed to confirm the existence of the cuspidal region, and to explore the rich dynamics associated with it.

This work was supported by DGICYT grant PB97-0685 and Generalitat de Catalunya grant 1999BEAI400103 (Spain).

REFERENCES

Ali, M. E. & Weidman, P. D. 1990 On the stability of circular Couette flow with radial heating. *J. Fluid Mech.* **220**, 53–84.

Becker, K. M. & Kaye, J. 1962 Measurements of diabatic flow in an annulus with a rotating inner cylinder. *Trans. ASME: C. J. Heat Transfer* **84**, 97–105.

Chida, K., Sakaguchi, S., Wagatsuma, M. & Kimura, T. 1982 High-speed coating of optical fibres with thermally curable silicone resin using a pressurized die. *Electronic Lett.* **18**, 713–715.

Chung, K. C. & Astill, K. N. 1977 Hydrodynamic instability of viscous flow between rotating coaxial cylinders with fully developed axial flow. *J. Fluid Mech.* **81**, 641–655.

Cotton, F. W. & Salwen, H. 1981 Linear stability of rotating Hagen–Poiseuille flow. *J. Fluid Mech.* **108**, 101–125.

Hart, J. E. 1971 Stability of the flow in a differentially heated inclined box. *J. Fluid Mech.* **47**, 547–576.

Hasoon, M. A. & Martin, B. W. 1977 The stability of viscous axial flow in an annulus with a rotating inner cylinder. *Proc. R. Soc. Lond.* A **352**, 351–380.

Joseph, D. D. 1976 *Stability of Fluid Motions*, vols I and II. Springer.

Ludwieg, H. Experimentelle Nachprufung des stabilitatstheorien fur reibungsfreie Stromungen mit schraubenlinienformigen stromlinien. *Z. Flugwiss.* **12**, 304–309.

Lueptow, R. M., Docter, A. & Min, K. 1992 Stability of axial flow in an annulus with a rotating inner cylinder. *Phys. Fluids* A **4**, 2446–2455.

Mackrodt, P. A. 1976 Stability of Hagen–Poiseuille flow with superimposed rigid rotation. *J. Fluid Mech.* **73**, 153–164.

Marques, F. & Lopez, J. M. 1997 Taylor–Couette flow with axial oscillations of the inner cylinder: Floquet analysis of the basic flow. *J. Fluid Mech.* **348**, 153–175.

McFadden, G. B., Coriell, S. R., Murray, B. T., Glicksman, M. E. & Selleck, M. E. 1990 Effect of a crystal–melt interface on Taylor-vortex flow. *Phys. Fluids* A **2**, 700–705.

Meseguer, A. & Marques, F. 2000 On the competition between centrifugal and shear instability in spiral Couette flow. *J. Fluid Mech.* **402**, 33–56.

Ollis, D. F. & Pelizzetti, E. & Serpone, N. 1991 Photocatalyzed destruction of water contaminants. *Environ. Sci. Technol.* **25**, 1523–1529.

Pearlstein, A. J. 1981 Effect of rotation on the stability of a doubly diffusive fluid layer. *J. Fluid Mech.* **103**, 389–412.

Tadmor, Z. & Bird, R. B. 1974 Rheological analysis of stabilizing forces in wire-coating dies. *Polymer Engng Sci.* **14**, 124–136.

Takeuchi, D. I. & Jankowski, D. F. 1981 A numerical and experimental investigation of the stability of spiral Poiseuille flow. *J. Fluid Mech.* **102**, 101–126; and corrigendum, **113**, 536 (referred to herein as TJ).